# Formation of renal cysts and tumors in Vhl/Trp53-deficient mice requires HIF-1 and HIF-2

Schönenberger, Désirée ; Harlander, Sabine ; Rajski, Michal ; Jacobs, Robert A ; Lundby, Anne-Kristine ; Adlesic, Mojca ; Hejhal, Tomas ; Wild, Peter J ; Lundby, Carsten ; Frew, Ian J

Abstract: The von Hippel-Lindau (VHL) tumor suppressor gene is inactivated in the majority of clear cell renal cell carcinomas (ccRCC), but genetic ablation of Vhl alone in mouse models is insufficient to recapitulate human tumorigenesis. One function of pVHL is to regulate the stability of the hypoxia-inducible factors (HIF), which become constitutively activated in the absence of pVHL. In established ccRCC, HIF-1 has been implicated as a renal tumor suppressor, whereas HIF-2 is considered an oncoprotein. In this study, we investigated the contributions of HIF-1 and HIF-2 to ccRCC initiation in the context of Vhl deficiency. We found that deleting Vhl plus Hif1a or Hif2a specifically in the renal epithelium did not induce tumor formation. However, HIF-1 and HIF-2 differentially regulated cell proliferation, mitochondrial abundance and oxidative capacity, glycogen accumulation, and acquisition of a clear cell phenotype in Vhl-deficient renal epithelial cells. HIF-1 , but not HIF-2 , induced Warburg-like metabolism characterized by increased glycolysis, decreased oxygen consumption, and decreased ATP production in mouse embryonic fibroblasts, providing insights into the cellular changes potentially occurring in Vhl mutant renal cells before ccRCC formation. Importantly, deletion of either Hif1a or Hif2a completely prevented the formation of renal cysts and tumors in Vhl/Tp53 mutant mice. These findings argue that both HIF-1 and HIF-2 exert pro-tumorigenic functions during the earliest stages of cyst and tumor formation in the kidney.

DOI: https://doi.org/10.1158/0008-5472.CAN-15-1859

**Formation of renal cysts and tumors in *Vhl/Trp53*-deficient mice requires HIF-1α and HIF-2α**

Désirée Schönenberger[1,#], Sabine Harlander[1,2,#], Michal Rajski[1,#], Robert A. Jacobs[1,2,3], Anne-Kristine Lundby[1,2], Mojca Adlesic[1], Tomas Hejhal[1], Peter J. Wild[4], Carsten Lundby[1,2] and Ian J. Frew[1,2]

[1] Institute of Physiology, University of Zurich, Zurich, Switzerland

[2] Zurich Center for Integrative Human Physiology, University of Zurich, Zurich, Switzerland

[3] Health and Physical Education, School of Teaching and Learning, Western Carolina University, North Carolina, USA

[4] Institute of Surgical Pathology, University Hospital Zurich, Zurich, Switzerland

[#] These authors contributed equally

**Running title**: HIF-1α and HIF-2α are renal oncogenes

**Key words:** clear cell renal cell carcinoma, mouse model, von Hippel-Lindau, hypoxia inducible factor, p53

**Financial support:** This work was supported by grants to I.J.F. from SNF Förderungsprofessur (PP00P3_128257), SNF NCCR Kidney.CH and ERC Starting Grant (260316).

**Corresponding author**:
Ian Frew
Institute of Physiology
University of Zurich
Winterthurerstrasse 190
CH-8057 Zurich
Switzerland
Phone: +41 44 635 5004
Fax: : +41 44 635 6814
Email: ian.frew@access.uzh.ch

**Conflict of interest:** The authors declare that there are no conflicts of interest related to this manuscript.

**ABSTRACT**

The von Hippel-Lindau (*VHL*) tumor suppressor gene is inactivated in the majority of clear cell renal cell carcinomas (ccRCC), but genetic ablation of *Vhl* alone in mouse models is insufficient to recapitulate human tumorigenesis. One function of pVHL is to regulate the stability of the hypoxia-inducible factors (HIF), which become constitutively activated in the absence of pVHL. In established ccRCC, HIF-1α has been implicated as a renal tumor suppressor, whereas HIF-2α is considered an oncoprotein. In this study, we investigated the contributions of HIF-1α and HIF-2α to ccRCC initiation in the context of *Vhl* deficiency. We found that deleting *Vhl* plus *Hif1a* or *Hif2a* specifically in the renal epithelium did not induce tumor formation. However, HIF-1α and HIF-2α differentially regulated cell proliferation, mitochondrial abundance and oxidative capacity, glycogen accumulation, and acquisition of a clear cell phenotype in *Vhl*-deficient renal epithelial cells. HIF-1α, but not HIF-2α, induced Warburg-like metabolism characterized by increased glycolysis, decreased oxygen consumption, and decreased ATP production in mouse embryonic fibroblasts, providing insights into the cellular changes potentially occurring in *Vhl* mutant renal cells before ccRCC formation. Importantly, deletion of either *Hif1a* or *Hif2a* completely prevented the formation of renal cysts and tumors in *Vhl/Tp53* mutant mice. These findings argue that both HIF-1α and HIF-2α exert pro-tumorigenic functions during the earliest stages of cyst and tumor formation in the kidney.

## INTRODUCTION

Clear cell renal cell carcinoma (ccRCC) is the most frequent renal malignancy and up to 92% of ccRCC tumors harbor biallelic inactivation of the von Hippel-Lindau (*VHL*) tumor suppressor gene (1). *VHL* mutations occur at the earliest stage of tumor formation (2). The absence of pVHL function is clearly necessary for the growth of fully transformed ccRCC cell lines as xenografts (3). However, the fact that the frequency of *VHL* mutant single epithelial cells vastly outweighs the number of ccRCC tumors in kidneys of familial VHL disease patients (4) and the absence of tumors in a variety of renal epithelial cell-specific *Vhl* knockout mice (reviewed in (5)) argues that ccRCC formation requires mutations in addition to *VHL*. There are currently no autochthonous mouse models that fully reproduce all of the characteristic morphological and invasive properties of human ccRCC, however, consistent with the hypothesis that multiple cooperating mutations are required for ccRCC development, kidney epithelial cell-specific co-deletion of *Vhl* with *Pten* (6), or with *Kif3a* to genetically ablate primary cilia (7), caused the formation of simple and atypical cystic lesions that are similar to the ccRCC precursor cystic lesions found in the kidneys of patients with inherited VHL disease. Deletion of *Vhl* together with homozygous loss of *Trp53* (8) or with heterozygous loss of *Bap1* (9), gave rise to very similar phenotypes, including simple and atypical cystic lesions as well as tumors containing cells that display cytoplasmic clearing and elevated mTORC1 activity, recapitulating many of the cellular and molecular changes that are characteristic of human ccRCC.

pVHL controls many biological activities including regulation of the stability of the hypoxia-inducible transcription factors α (HIF-1α, HIF-2α and HIF-3α, collectively HIF-α) (10), regulation of NF-κB activity (11), maintenance of the primary cilium (12), activation of p53 (13), secretion of extracellular matrix components (14), promotion of DNA double strand repair (15), regulation of the plane of cellular division (16,17) and suppression of aneuploidy (16,18). The combined loss of several or all of pVHL's functions could contribute to tumor initiation and progression. Loss of

function mutations of *VHL* occur in ccRCC mutually exclusively to rarer mutations in *TCEB1*, encoding Elongin C, and collectively these cause constitutive stabilization of HIF-α in up to 95% of ccRCC tumors (1), implying that HIF-α activation is a major oncogenic driving force in ccRCC. HIF-1α and HIF-2α appear to play opposite roles in determining the aggressiveness of established ccRCCs; HIF-1α inhibits, whereas HIF-2α promotes tumor formation in ccRCC xenografts (19-21), copy loss of the chromosomal locus harboring the *HIF1A* gene predicts poor patient outcome (22) and sporadic ccRCCs expressing HIF-1α and HIF-2α exhibit lower proliferation rates than ccRCCs expressing only HIF-2α (23). ccRCC cell lines frequently express only HIF-2α and do not express functional HIF-1α due to biallelic alterations of the *HIF1A* locus (24). Knockdown of *HIF1A* in ccRCC cell lines that express both HIF-1α and HIF-2α promotes xenograft tumor formation (24). These studies argue that whereas HIF-2α activity is tumor promoting, there is a selection against HIF-1α expression or activity during the progression of some cases of ccRCC. On the other hand, the observations that HIF-1α is strongly expressed in single and multicellular clusters of *VHL* null cells and in cystic lesions in VHL patients (4), transgenic overexpression of Hif-1α in mouse proximal tubular epithelial cells causes a clear cell appearance, increased proliferation and a disorganized tubular morphology (25) and many human ccRCCs express HIF-1α and HIF-1α target genes (26), it may also be argued that HIF-1α plays an important role in promoting ccRCC development. These studies have largely focused on fully transformed, genetically complex ccRCC cell lines derived from advanced tumors and it remains unclear if and how HIF-1α and HIF-2α contribute to the earliest stages of initiation of ccRCC.

An early event following *VHL* mutation is likely to be a profound alteration of cellular metabolic pathways. Numerous HIF-1α and/or HIF-2α-dependent metabolic changes occur in ccRCC cell lines, including elevated glucose uptake and conversion to lactate with a concomitant reduction in mitochondrial oxidation of pyruvate, reduced mitochondrial biogenesis, reduced mitochondrial

complex I activity, altered cytochrome c oxidase activity, increased pentose phosphate pathway flux, decreased oxidative glutaminolysis and increased lipogenesis through reductive glutamine metabolism (27-38). Since ccRCC cell lines have complex genetic backgrounds that arose during tumor evolution, it is possible that some of these metabolic changes might be driven by late-occurring mutations that further modify metabolic pathways and allow ccRCC cells to proliferate efficiently in the metabolic environment imposed by constitutive HIF-α activity. For example, ccRCCs can harbor activating mutations in the PI3K-mTORC1 pathway, inactivating *TP53* mutations or can exhibit high levels of MYC expression or decreased FBP expression (1,38,39), all of which are known to influence numerous cellular metabolic pathways. The metabolic alterations that follow *VHL* mutation in otherwise genetically normal renal epithelial cells at the start of the process of tumor formation remain unclear.

Given the importance of HIF-1α and HIF-2α in ccRCC, we asked whether the loss or constitutive activation of HIF-1α or HIF-2α alters renal epithelial proliferative homeostasis, metabolism and the initiation of renal cysts and tumours by undertaking a systematic approach of genetic deletion of *Hif1a* or *Hif2a* alone, together with *Vhl* and together with *Vhl*/*Trp53* in renal epithelial cells in mice.

## MATERIALS AND METHODS

### Mouse strains

*Hif1a*$^{fl/fl}$ (40) and *Hif2a*$^{fl/fl}$ (41) mice were crossed with *Ksp1.3-Cre;Vhl*$^{fl/fl}$ (6), *Ksp1.3-Cre;Vhl*$^{fl/fl}$*;Trp53*$^{fl/fl}$ (8) or *Ksp1.3-Cre/+* (42) mice. Littermate mice that lacked the Cre transgene served as wild type controls.

### Immunohistochemistry

Immunohistochemistry and immunofluorescence of formalin fixed paraffin embedded tissues was performed as previously described (6,8) using antibodies listed in Supplementary Materials and Methods.

### Respirometry

Biopsies (1 $mm^3$) of renal cortex and medulla were assayed for oxygen consumption following the addition of different respiratory substrates and inhibitors using high-resolution respirometry (Oxygraph-2k, ORBOROS INSTRUMENTS Corp, Innsbruck, Austria) according to the protocol described in Supplementary Materials and Methods.

### Microarrays

Primary adult mouse renal epithelial cells were cultured for 3 days and infected with Adeno-GFP (Vector Biolabs, 1060) or Adeno-Cre (Vector Biolabs, 1700) as described (8). mRNA was isolated 4 days after adenovirus infection and Cy3- and Cy5-labelled cDNA from GFP- and Cre-samples was competitively hybridised to Mouse GE 4x44K v2 Microarrays (Agilent). Dye swap experiments were used to control potential dye-specific hybridisation effects. Analysis using R/Bioconductor package limma was based on the average fold expression level changes (Cre/GFP) of three independent biological experiments. MIAME compliant microarray data are accessible through GEO number GSE75745.

**Histological stains**

H&E and PAS stains were conducted using standard protocols. For the visualization of lipids, frozen kidney sections were fixed with 10% formalin for 15 min, washed in tap water, equilibrated in 60% isopropanol and stained with Oil red O (3 mg/ml in 60% isopropanol) overnight at 4 °C. After rinsing in 60% isopropanol, sections were washed with water, counterstained with hematoxylin and mounted in Mowiol.

**Real time PCR**

RNA isolation, cDNA preparation and real time PCR were performed as described (6) using primers listed in Supplemental Materials and Methods.

**Mouse embryo fibroblasts (MEFs)**

MEFs were isolated from E13.5 embryos of relevant non-Cre expressing floxed mouse strains or C57BL/6 embryos (for wild type MEFs) and cultured as previously described (8) at 5% $O_2$ and 5% $CO_2$. MEFs were infected with adenovirus expressing Cre recombinase and GFP (Ad-Cre-GFP, Vector Biolabs, #1700) or GFP only (Ad-CMV-GFP, Vector Biolabs #1060). Detailed protocols for measuring ATP, ECAR, OCR, lactate production, glucose utilization and mitochondrial content are described in Supplementary Materials and Methods.

**Statistical analyses**

Unless otherwise stated, data are presented as mean ± std. dev. and statistical differences assessed using Student's unpaired *t*-test. *, **, and *** denote $p < 0.05$, $p < 0.01$ and $p < 0.001$ respectively.

## RESULTS

### *Vhl* deletion together with deletion of *Hif1a* or *Hif2a* does not cause renal tumors

Most cases of ccRCC appear to arise from the proximal tubule although there is also evidence that some cases can arise from cells in other nephron segments (5). We employed the *Ksp1.3-Cre* transgene that induces epithelial cell-specific gene deletion widely throughout different segments of the nephron, including in a significant number of proximal tubular cells, as well as in epithelia of several genital tract tissues (42). We generated *Ksp1.3-Cre;Vhl*$^{fl/fl}$ (Vhl$^{\Delta/\Delta}$) (6), *Ksp1.3-Cre;Hif1a*$^{fl/fl}$ (Hif1a$^{\Delta/\Delta}$), *Ksp1.3-Cre;Hif2a*$^{fl/fl}$ (Hif2a$^{\Delta/\Delta}$), *Ksp1.3-Cre;Vhl*$^{fl/fl}$*;Hif1a*$^{fl/fl}$ (Vhl$^{\Delta/\Delta}$Hif1a$^{\Delta/\Delta}$) and *Ksp1.3-Cre;Vhl*$^{fl/fl}$*;Hif2a*$^{fl/fl}$ (Vhl$^{\Delta/\Delta}$Hif2a$^{\Delta/\Delta}$) mice to achieve renal epithelial-specific loss or constitutive stabilization of HIF-1α and/or HIF-2α (Fig. 1A and B). Immunohistochemical staining confirmed the expected stabilization of either or both HIF-1α and HIF-2α in the relevant *Vhl* mutant genotypes (Fig. 1C and D). All of the above-described mutant mice were analysed at 6, 12 and 18 months of age. Neither *Hif1a* nor *Hif2a* deletion alone had any effect on the morphology of kidneys. *Vhl/Hif1a* double deletion, but not *Vhl/Hif2a* double deletion, fully rescued (data not shown) the previously-reported hydronephrosis phenotype caused by *Vhl* deletion (6). This phenotypic rescue will be described in detail elsewhere. Vhl$^{\Delta/\Delta}$ mice do not develop ccRCC precursor lesions or tumors (6). We reasoned that HIF-1α might act as an anti-proliferative factor that prevents tumor development following *Vhl* mutation. However, none of the genotypes exhibited cysts, dysplastic lesions or tumors in the cortex, medulla or papilla even when aged for 18 months. Tubular epithelial cells in Vhl$^{\Delta/\Delta}$Hif2a$^{\Delta/\Delta}$ mice frequently displayed a highly unusual "optically-clear" nucleus, characterised by a thin ring of chromatin surrounding a non-stained region in the centre (Supplementary Fig. S1). Papillary thyroid carcinomas display optically clear nuclei but this histological feature does not arise in ccRCCs. We conclude that the combination of loss of the many putative tumor suppressor functions of pVHL plus constitutive expression of the putative oncoprotein HIF-2α plus the absence of the putative tumor suppressor activity of HIF-1α does not cause cyst or tumor initiation.

**_Hif1a_ and _Hif2a_ are both necessary for renal cyst and tumor formation caused by _Vhl/Trp53_ deletion**

We next investigated potential requirements for *Hif1a* or *Hif2a* in the initiation of renal cysts and tumors in the *Vhl/Trp53* double mutant background (8). We generated *Ksp1.3-Cre;Vhl$^{fl/fl}$;Trp53$^{fl/fl}$;Hif1a$^{fl/fl}$* (Vhl$^{\Delta/\Delta}$Trp53$^{\Delta/\Delta}$Hif1a$^{\Delta/\Delta}$) and *Ksp1.3-Cre;Vhl$^{fl/fl}$;Trp53$^{fl/fl}$;Hif2a$^{fl/fl}$* (Vhl$^{\Delta/\Delta}$Trp53$^{\Delta/\Delta}$Hif2a$^{\Delta/\Delta}$) mice (Fig. 2A,B) and confirmed HIF-1α and HIF-2α stabilization in the relevant genotypes (Fig. 2C and D). PCRs specific for the recombined *Vhl* and *Trp53* alleles demonstrated that these genes were deleted efficiently in these mice (Supplementary Fig. S2). We analyzed cohorts at 6 and 12 months of age. Table 1 shows a summary of the incidence of different phenotypes in each genotype and Fig. 2 shows examples of these phenotypes. We previously demonstrated (8) that Vhl$^{\Delta/\Delta}$Trp53$^{\Delta/\Delta}$ mice display hydronephrosis, seminal vesicle developmental abnormalities (Fig. 2F), sub-fertility and sub-viability and by 12 months of age these mice develop simple and atypical kidney cysts (Fig. 2B), kidney tumors (Fig. 2F), disorganized and multilayered epididymal epithelial cell growth (Fig. 2G), epididymal squamous metaplasia (Fig. 2H) and benign epididymal tumors at high penetrance. About one third of these mice also develop a variety of genital-urinary tract carcinomas (8). All of these phenotypes were completely absent in Vhl$^{\Delta/\Delta}$Trp53$^{\Delta/\Delta}$Hif1a$^{\Delta/\Delta}$ mice. Six month-old Vhl$^{\Delta/\Delta}$Trp53$^{\Delta/\Delta}$ mice frequently displayed disorganized renal tubular epithelia with a clear cell appearance but this phenotype was not present in Vhl$^{\Delta/\Delta}$Trp53$^{\Delta/\Delta}$Hif1a$^{\Delta/\Delta}$ mice (Fig. 2A). These mice developed only a few micro-cysts at a frequency that was not higher than littermate control mice (data not shown) and importantly no large renal cysts or tumors arose in mice aged 12 months (Fig. 2B, Table 1). Epididymides of Vhl$^{\Delta/\Delta}$Trp53$^{\Delta/\Delta}$Hif1a$^{\Delta/\Delta}$ mice displayed nuclear atypia and mild epithelial disorganization (Fig. 2G and H), similar to the phenotypes observed in younger Vhl$^{\Delta/\Delta}$Trp53$^{\Delta/\Delta}$ mice (8) but did not develop epithelial dysplasia or squamous metaplasia. No malignant tumors were observed in any other genital-urinary tract organs in these mice (Table 1). Thus, HIF-1α activity is indispensible for the

initiation of kidney cyst and tumor formation and for the formation of genital-urinary tract malignancies.

In contrast, $Vhl^{\Delta/\Delta}Trp53^{\Delta/\Delta}Hif2a^{\Delta/\Delta}$ mice displayed several identical phenotypes to $Vhl^{\Delta/\Delta}Trp53^{\Delta/\Delta}$ mice, including hydronephrosis (data not shown), seminal vesicle developmental abnormalities (Fig. 2F), disorganized epididymal epithelial growth (Fig. 2G) and epididymal squamous metaplasia (Fig. 2H), although these epididymal phenotypes were present in only half of the mice (Table 1) and were much smaller lesions than those seen in $Vhl^{\Delta/\Delta}Trp53^{\Delta/\Delta}$ mice. Similarly to $Vhl^{\Delta/\Delta}Trp53^{\Delta/\Delta}$ mice, $Vhl^{\Delta/\Delta}Trp53^{\Delta/\Delta}Hif2a^{\Delta/\Delta}$ mice were also sub-fertile and sub-viable, with many mice dying at various ages, possibly due to kidney failure caused by excessive hydronephrosis. While 6 month-old $Vhl^{\Delta/\Delta}Trp53^{\Delta/\Delta}Hif2a^{\Delta/\Delta}$ mice displayed disorganized renal tubular epithelia with optically-clear nuclei (Fig. 2A), no large renal cysts or tumors (Fig. 2B), nor genital-urinary tract carcinomas were observed in 12 month-old mice. Thus, many of the pre-neoplastic and all of the neoplastic phenotypes resulting from combined deletion of *Vhl* and *Trp53* are also dependent on HIF-2α activity.

**HIF-1α and HIF-2α both contribute to increased cellular proliferation in *Vhl* and *Vhl/Trp53* mutant mice**

Since HIF-1α and HIF-2α have been implicated in regulating the proliferation of ccRCC cells, we analysed the roles of HIF-1α and HIF-2α in proliferative control in mouse renal epithelia. Ki67 staining to label proliferating epithelial cells in the renal cortex revealed that tubules in 6 month-old *Vhl* knockout mice displayed an increased number of proliferating cells. This phenotype was completely rescued by co-deletion of *Hif1a* and partially rescued by co-deletion of *Hif2a* (Fig. 3A and C), indicating a major and minor role of HIF-1α and HIF-2α, respectively, in causing increased cellular proliferation. We next asked whether the rescue of cyst and tumour formation in the *Vhl/Trp53* mutant background was due to a requirement for HIF-1α or HIF-2α in causing enhanced

proliferation. In fact, Ki67 labelling revealed elevated numbers of proliferating epithelial cells in the renal cortices of 12 month-old $Vhl^{\Delta/\Delta}Trp53^{\Delta/\Delta}$, $Vhl^{\Delta/\Delta}Trp53^{\Delta/\Delta}Hif1a^{\Delta/\Delta}$ and $Vhl^{\Delta/\Delta}Trp53^{\Delta/\Delta}Hif2a^{\Delta/\Delta}$ mice in comparison to littermate control mice (Fig. 3B and D) indicating that increased cellular proliferation is not the sole cause of cyst and tumor formation. Inter-genotype comparisons revealed that deletion of either *Hif1a* or *Hif2a* lowered proliferation in the *Vhl/Trp53* mutant background with loss of *Hif1a* causing a stronger decrease in proliferation than loss of *Hif2a*. The absence of a complete rescue by *Hif1a* deletion in the *Vhl/Trp53* mutant background, in comparison to the complete rescue in the *Vhl* mutant background, argues that loss of *Trp53* also contributes to increased proliferation in the *Vhl/Trp53* mutant background.

**HIF-1α regulates glycolysis, oxidative metabolism and mitochondrial abundance in renal epithelial cells**

To gain further molecular insights into HIF-1α- and HIF-2α-dependent processes in *Vhl* null cells that might be necessary for tumor initiation, we developed a system to culture primary renal epithelial cells derived from kidneys of adult $Vhl^{fl/fl}$, $Vhl^{fl/fl}Hif1a^{fl/fl}$, $Vhl^{fl/fl}Hif2a^{fl/fl}$ and $Vhl^{fl/fl}Hif1a^{fl/fl}Hif2a^{fl/fl}$ mice. Epithelial morphology (Supplementary Fig. S3A), *Cdh1* mRNA expression (Supplementary Fig. S3B) and E-Cadherin protein expression (Supplementary Fig. S3C) were maintained for at least 12 days of culture, implying that the epithelial phenotype of these cells is largely preserved in this culture system. Cultures were infected with adenovirus expressing GFP as control or with adenovirus expressing Cre (Fig. 4A) and real time PCR confirmed the deletion of the floxed genes (Supplementary Fig. S3D). Microarray comparisons of global mRNA expression 4 days after viral infection revealed a transcriptional signature induced by loss of *Vhl* that included 753 probes that were significantly ($p < 0.05$) upregulated more than 1.5 fold and 451 probes downregulated more than 1.5 fold. This transcriptional signature was used to probe mRNA expression data derived from human normal kidney and ccRCC samples (GSE17895). Unsupervised clustering using the *Vhl*-deletion gene signature accurately segregated human

ccRCCs from normal kidney tissue (Supplementary Fig. S4), demonstrating that our culture system can identify ccRCC-relevant gene expression changes. We identified genes that were upregulated by loss of *Vhl* and that were dependent solely on *Hif1a* or solely on *Hif2a* or that remained upregulated when either *Hif1a* or *Hif2a* were deleted but not when both were deleted, indicating that they are targets of both HIF-1α and HIF-2α (Fig. 4B, Supplementary Table S1). While the *Hif2a*-dependent and *Hif1a/Hif2a*-dependent gene sets were not strongly enriched for sets of genes that participate in particular biological processes, the *Hif1a*-dependent target genes (Fig. 4C) encompassed numerous previously-identified hypoxia and HIF-α-targets (*Bnip3*, *Bnip3l*, *Egln3*, *Loxl2*, *Ak4*, *Car9*, *Vegfa*, *P4ha2, Mif*), including genes that regulate cellular metabolism (Supplementary Fig. S5) by promoting glycolytic flux (*Slc2a1*, *Gpi1, Pfkl, Pfkfb3*, *Aldoa*, *Aldoc, Tpi1, Gapdh*, *Pgk1*, *Pgam1*, *Eno1*), promoting glycogenolysis (*Pygl*, *Pgm2*), diverting glucose-derived carbon from mitochondrial oxidation to lactate production and excretion (*Pdk1*, *Ldha*, *Slc16a3*) or regulating mitochondrial electron transport by inhibiting complex I (*Ndufa4l2*) (36). Real time PCR analyses of mRNA isolated from $Vhl^{\Delta/\Delta}$, $Vhl^{\Delta/\Delta}Hif1a^{\Delta/\Delta}$ and $Vhl^{\Delta/\Delta}Hif2a^{\Delta/\Delta}$ kidneys confirmed that several of these gene expression changes (*Pgk1*, *Pdk1*, *Pfkfb3*, *Ldha*, *Ndufa4l2*), as well as upregulation of *Cox4-2*, which alters the efficiency of cytochrome c oxidase (37), also occur upon *Vhl* deletion *in vivo* and demonstrated that, with the exception of *Ndufa4l2*, all were strictly dependent on *Hif1a* and independent of *Hif2a* (Fig. 4D). A similar *Hif1a*-dependent, *Hif2a*-independent metabolic gene expression signature was observed in cultured primary renal epithelial cells (Supplementary Fig. S6A,B) and kidneys (Supplementary Fig. S6C) in the *Vhl/Trp53* double mutant background, indicating that the induction of expression of these genes is independent of p53 function. Moreover, elevated GLUT1 protein expression was detected in renal tubules in $Vhl^{\Delta/\Delta}$, $Vhl^{\Delta/\Delta}Trp53^{\Delta/\Delta}$, $Vhl^{\Delta/\Delta}Hif2a^{\Delta/\Delta}$ and $Vhl^{\Delta/\Delta}Trp53^{\Delta/\Delta}Hif2a^{\Delta/\Delta}$ mice but not in $Vhl^{\Delta/\Delta}Hif1a^{\Delta/\Delta}$ or $Vhl^{\Delta/\Delta}Trp53^{\Delta/\Delta}Hif1a^{\Delta/\Delta}$ mice (Figs. 1E and 2E).

Since this *Hif1a*-activated transcriptional signature predicted decreased flux of pyruvate into mitochondria and decreased mitochondrial electron transport (Supplementary Fig. S5), we developed a method to analyse mitochondrial respiration in biopsies of the renal cortex and medulla. Oxygen consumption resulting from various steps of mitochondrial oxidation was assessed by sequential addition of the following metabolic intermediates or inhibitors; i) malate, octanoyl-carnitine and ADP to determine medium chain fatty acid oxidation, ii) pyruvate and glutamate to determine complex I-specific activity, iii) succinate to determine total ATP synthase capacity, iv) rotenone to inhibit complex I and determine complex II-specific activity, v) antimycin A to block complex III, allowing the correction of residual $O_2$ consumption and vi) TMPD and ascorbate to determine maximal cytochrome c oxidase activity (complex IV). *Vhl* deletion caused a decrease in all of the assays of respiratory capacity in the medulla but not cortex of these mice (Fig. 4E), consistent with the fact that the majority of tubules in the medulla are null for *Vhl* and the fact that proximal tubular cells, where gene deletion occurs in a minority of cells, are the most abundant cell type in the cortex. These effects were completely rescued in $Vhl^{\Delta/\Delta}Hif1a^{\Delta/\Delta}$ but not $Vhl^{\Delta/\Delta}Hif2a^{\Delta/\Delta}$ kidneys (Fig. 4E), consistent with the *Hif1a*-dependency of the gene expression changes. Since HIF-1α has been shown to decrease mitochondrial abundance via multiple mechanisms (32,43), we analysed mitochondrial abundance in AQP2 expressing collecting duct principal cells using immunofluorescence for the mitochondrial outer membrane protein TOM20. Reduced TOM20 staining intensity was observed in these cells in $Vhl^{\Delta/\Delta}$ and in $Vhl^{\Delta/\Delta}Hif2a^{\Delta/\Delta}$ kidneys, whereas $Vhl^{\Delta/\Delta}Hif1a^{\Delta/\Delta}$ kidneys exhibited increased TOM20 staining (Fig. 5A-H and U), consistent with the measures of cellular respiration. Similar results were obtained in the *Vhl/Trp53* mutant background (Supplementary Fig. S7E-M). We conclude that HIF-1α but not HIF-2α stabilization decreases mitochondrial abundance and oxidative capacity independently of p53 function in *Vhl* mutant renal tubular cells *in vivo*.

We next investigated whether the characteristic clear cell phenotype of ccRCC, believed to be caused by the cytoplasmic accumulation of lipids and glycogen, was also dependent on *Hif1a*. Indeed, tubular epithelial cells in $Vhl^{\Delta/\Delta}$, $Vhl^{\Delta/\Delta}Trp53^{\Delta/\Delta}$, $Vhl^{\Delta/\Delta}Hif2a^{\Delta/\Delta}$ and $Vhl^{\Delta/\Delta}Trp53^{\Delta/\Delta}Hif2a^{\Delta/\Delta}$ mice, but not in $Vhl^{\Delta/\Delta}Hif1a^{\Delta/\Delta}$ and $Vhl^{\Delta/\Delta}Trp53^{\Delta/\Delta}Hif1a^{\Delta/\Delta}$ mice frequently demonstrated clear cell morphology (Fig. 5I-L and 2A-D). Tubules in $Hif1a^{\Delta/\Delta}$ and $Hif2a^{\Delta/\Delta}$ mice did not display morphological alterations (Supplementary Fig. S1). Tubules in $Vhl^{\Delta/\Delta}$, $Vhl^{\Delta/\Delta}Trp53^{\Delta/\Delta}$, $Vhl^{\Delta/\Delta}Hif1a^{\Delta/\Delta}$, $Vhl^{\Delta/\Delta}Trp53^{\Delta/\Delta}Hif1a^{\Delta/\Delta}$, $Vhl^{\Delta/\Delta}Hif2a^{\Delta/\Delta}$ and $Vhl^{\Delta/\Delta}Trp53^{\Delta/\Delta}Hif2a^{\Delta/\Delta}$ kidneys all displayed strong accumulation of cytoplasmic glycogen droplets as assessed by periodic acid-Schiff (PAS) staining (Fig. 5M-P, Supplementary Fig. S7A-D) and the optically-clear nuclei in $Vhl^{\Delta/\Delta}Hif2a^{\Delta/\Delta}$ and $Vhl^{\Delta/\Delta}Trp53^{\Delta/\Delta}Hif2a^{\Delta/\Delta}$ mice also displayed strong glycogen accumulation (Fig. 5P, Supplementary Fig. S7D), which may be the cause of this phenotype. While several genes encoding enzymes of glycogenolysis and glycogen synthesis were upregulated in *Vhl* deficient kidneys, these gene expression changes were abolished by co-deletion of either *Hif1a* or *Hif2a* (Fig. 5W), suggesting that this is not the cause of glycogen accumulation. Surprisingly, no accumulation of lipids was observed in tubular cells in any genotype, as assessed by Oil red O (Fig. 5Q-T) and Nile red (data not shown) stainings. Peri-renal fat in the same samples served as positive control for these stainings (Fig. 5V). Thus, while HIF-1α-dependent reductions in mitochondrial abundance and oxidative capacity correlate with the presence of a clear cell cytoplasm, neither glycogen nor lipid accumulation appear to be the cause of this phenotype.

**HIF-1α induces reduced cellular ATP levels in *Vhl* deficient cells independently of p53**

We next turned to a primary cell culture-based system to gain more insight at the cellular level into the metabolic alterations that follow *Vhl* deletion. Since primary renal tubular epithelial cells rapidly de-differentiate after trypsinisation they were not suitable for these experiments. We instead utilized primary mouse embryo fibroblasts (MEFs) as a genetically tractable cell culture system and focused on alterations in glucose metabolism and oxygen consumption. We derived MEFs from

*Vhl*$^{fl/fl}$, *Vhl*$^{fl/fl}$*Hif1a*$^{fl/fl}$, *Vhl*$^{fl/fl}$*Hif2a*$^{fl/fl}$ and *Vhl*$^{fl/fl}$*Hif1a*$^{fl/fl}$*Hif2a*$^{fl/fl}$ embryos and infected them with adenoviruses expressing GFP (Adeno-GFP) or Cre (Adeno-Cre). The efficient deletion of all genes in the relevant floxed genotypes was confirmed by real time PCR (Supplementary Fig. S8). We investigated the dependence on *Hif1a* and *Hif2a* of the expression of a series of the key HIF-1α-dependent metabolic genes that we identified in renal epithelial cells. The mRNA levels of *Slc2a1*, *Pfkfb3*, *Pgk1*, *Ldha*, *Pdk1*, *NduFa4l2* and *Cox 4-2* were elevated in *Vhl* mutant cells in a *Hif1a*-dependent but *Hif2a*-independent manner (Fig. 6A), identically to the results seen in primary renal epithelial cells and in knockout kidneys. Deletion of *Vhl* induces premature senescence that can be rescued by co-deletion of *Trp53* (8). *Vhl/Trp53* double null MEFs also exhibited higher mRNA abundance of these genes (Fig. 6A), indicating that the gene expression pattern is not a secondary consequence of senescence, nor is it dependent on p53. Since this gene expression pattern is expected to promote the conversion of glucose-derived pyruvate into lactate at the expense of entry of pyruvate into the mitochondria for oxidative phosphorylation, we analysed cellular readouts of glycolytic flux in cells cultured at 20% $O_2$. Modest increases in glucose utilization (Fig. 6B) and extracellular acidification rate (Fig. 6C), as well as increases in the amount of lactate secreted by the cells (Fig. 6D), were observed in *Vhl* and *Vhl/Trp53* null MEFs. In contrast to these relatively small increases, there was a large decrease in oxygen consumption (Fig. 6E) in *Vhl* and *Vhl/Trp53* null MEFs that was not attributable to reduced mitochondrial mass, as assessed by NAO staining (Fig 6F). These results show that *Vhl* deletion causes a modest increase in glucose uptake and conversion to lactate but a large decrease in the activity of the mitochondrial TCA cycle, reflected by a lowered oxygen consumption rate. The reduced levels of oxidative phosphorylation that are not compensated by a large elevation in glucose flux to lactate suggested that cells may not be able to produce normal levels of ATP. Indeed, *Vhl* and *Vhl/Trp53* deletion caused a decrease in cellular ATP levels (Fig. 6G) that is dependent on *Hif1a* but independent of *Hif2a* (Fig. 6H), consistent with the transcriptional effects of these gene deletions on metabolic regulatory genes.

**DISCUSSION**

The molecular and cellular causes of ccRCC are incompletely understood. Biallelic inactivation of *VHL* is an early event in most ccRCCs but deletion of *Vhl* in renal epithelial cells in mice does not cause tumor formation (5). Correlative and functional genetic studies of human ccRCC have demonstrated that HIF-1α stabilization exerts a tumor suppressor-like activity while HIF-2α behaves oncogenically in the context of tumor cell proliferation (5). Here we tested the hypothesis that abolishing HIF-1α stabilization might allow hyperproliferation of *Vhl* mutant kidney epithelial cells *in vivo*, potentially allowing cysts or ccRCC tumors to form. In fact, *Hif1a* co-deletion rescued the increased epithelial cell turnover caused by *Vhl* deletion and $Vhl^{\Delta/\Delta}Hif1a^{\Delta/\Delta}$ mice developed no renal proliferative abnormalities. Similar mouse models in which *Vhl* and *Hif1a* were deleted in renal epithelial cells under the control of different nephron segment-specific Cre transgenes also did not lead to tumor formation (44,45). Our $Vhl^{\Delta/\Delta}Hif2a^{\Delta/\Delta}$ mice similarly did not develop renal cysts or tumors. Thus, despite the numerous putative tumor suppressor functions of *Vhl*, its deletion together with constitutive stabilization of HIF-1α and HIF-2α alone or together are insufficient for renal tumor formation. Previous studies employing various strategies to achieve HIF-1α and/or HIF-2α activation in *Vhl* wild type renal epithelia also failed to induce tumor formation beyond the stage of simple cysts or small dysplastic lesions (25,46-48). *Vhl/Trp53* deletion leads to the formation of simple and atypical renal cysts, renal tumors as well as carcinomas in other organs of the genital tract (8). We anticipated that the tumor phenotype in these mice might be enhanced by *Hif1a* co-deletion. In fact, all phenotypes in these mice were completely rescued. Similarly, co-deletion of *Hif2a* in this genetic background also completely prevented the formation of renal cysts, renal tumors and malignancies of the genital-urinary tract. Insofar as the *Vhl/Trp53* deletion model mimics the initial stages of evolution of ccRCCs, these findings demonstrate that HIF-1α and HIF-2α stabilization both play essential oncogenic roles in cyst and tumor formation. It will be interesting in further mouse genetic studies to determine whether HIF-1α and HIF-2α are also both

necessary for the formation of tumors induced by other mutations that cooperate with *Vhl*, such as *Bap1* (9).

It seems likely that HIF-1α and HIF-2α might each alter multiple cellular processes that are separately or cooperatively necessary for cyst and tumor evolution. While our studies uncoupled increased epithelial turnover from cyst and tumor formation, we identified several metabolic alterations that precede tumor formation. In *Vhl* mutant renal epithelial cells, HIF-1α induces a transcriptional program that promotes the glycolytic conversion of glucose to lactate and decreases mitochondrial oxidation of glucose- and fatty acid-derived carbons. HIF-1α also decreased the abundance of mitochondria in collecting duct epithelial cells, consistent with previous findings in cultured human cells that HIF-1α decreases mitochondrial biogenesis via MXI1-MYC-PGC1β and increases mitophagy via BNIP3 (32,43). Our microarray observation that *Bnip3* expression is upregulated in *Vhl* deficient renal epithelial cells (Fig. 4C) provides the basis for future studies to uncover how *Vhl* loss reduces mitochondrial abundance. In established ccRCC cell lines, increasing mitochondrial abundance by constitutive PGC-1α expression causes decreased xenograft tumor growth (49), consistent with our correlative data that $Vhl^{\Delta/\Delta}Trp53^{\Delta/\Delta}Hif1a^{\Delta/\Delta}$ mice do not show decreases in mitochondrial abundance and activity and do not develop cysts or tumors. These findings argue that a reduction in mitochondrial abundance promotes tumorigenesis. On the other hand, we show in MEFs that HIF-1α induces Warburg-like metabolism associated with increased conversion of glucose to lactate, decreased mitochondrial oxygen consumption and a lowered cellular level of ATP, implying that reduced cellular ATP levels may be an early cellular consequence of *VHL* gene deletion. The role that this mode of metabolism might play in promoting or inhibiting ccRCC formation remains to be determined but it is noteworthy in human ccRCCs that high mRNA expression levels of several of the HIF-1α-dependent metabolic genes that we identify in this study (including *PFKM*, *ALDOB*, *PGK1*, *PGM2*, *ENO1*, *LDHA*, *PDK1*), as well as higher levels of phosphorylated AMPK, a predicted consequence of HIF-1α-mediated reduction in cellular

ATP levels, correlate with better patient outcome (39). This finding argues that the HIF-1α metabolic transcriptional signature acts to restrain aggressive tumor behavior. Thus, it appears that different metabolic activities of HIF-1α may contribute differently to different aspects of tumor formation and progression. Additionally, it appears likely that mutations or alterations in the expression of other metabolism-regulating genes, such as decreased expression of FBP (38), may act together with HIF-1α to further alter cellular metabolic pathways to achieve a balance of high rates of glycolytic and pentose phosphate pathway flux and sufficient oxidative phosphorylation to provide the necessary metabolic intermediates and ATP to fuel efficient biosynthesis, cellular proliferation and tumor growth.

*VHL* mutant "normal" tubular cells in VHL patient kidneys exhibit clear cell morphology (4), highlighting that this phenotype precedes tumor formation. We demonstrate that HIF-1α stabilization but not HIF-2α stabilization induces the clear cell phenotype, consistent with previous observations based on overexpression of stabilized mutants of HIF-1α and HIF-2α (25,48). Somewhat surprisingly, while decreased mitochondrial activity and abundance correlated with the presence of clear cell cytoplasm, the accumulation of glycogen deposits did not and renal tubules did not accumulate lipids. These findings contradict the widely-held idea that the clear cell phenotype results from cytoplasmic lipid and glycogen accumulation.

Our studies encourage a modification of the idea that HIF-2α is the ccRCC oncogene and that HIF-1α restrains tumor progression. We argue that while activation of HIF-1α or HIF-2α alone or together are insufficient for tumor formation following biallelic inactivation of *VHL*, their activities are each indispensible for the formation of cysts and tumors that arise as a consequence of cooperating secondary mutations. The frequent selection in human ccRCC for functional losses of the *HIF1A* gene (24) or for other post-transcriptional alterations that impair HIF-1α stability and promote HIF-2α activity (50) raises the intriguing idea that HIF-1α may switch during tumor

evolution from being a factor that is initially necessary for tumor formation (oncogene) to one that later restrains tumor progression (tumor suppressor). Our findings also raise the idea that pharmacological inhibition of either HIF-1α or HIF-2α may be sufficient to prevent ccRCC formation in patients with inherited *VHL* mutations.

**ACKNOWLEDGEMENTS**

We are grateful to Strahil Georgiev and Wilhelm Krek for providing *Vhl*$^{fl/fl}$*Hif1a*$^{fl/fl}$ and *Vhl*$^{fl/fl}$*Hif2a*$^{fl/fl}$ mice, to the Centre for Microscopy and Image Analysis (UZH) and to Tatiana Simka for assistance with SeaHorse assays.

**References**


1. Sato Y, Yoshizato T, Shiraishi Y, Maekawa S, Okuno Y, Kamura T, et al. Integrated molecular analysis of clear-cell renal cell carcinoma. *Nature Genetics*. 2013;**45**:860–7.

2. Gerlinger M, Horswell S, Larkin J, Rowan AJ, Salm MP, Varela I, et al. Genomic architecture and evolution of clear cell renal cell carcinomas defined by multiregion sequencing. *Nature Genetics*. 2014;**46**:225–33.

3. Iliopoulos O, Kibel A, Gray S, Kaelin WG. Tumour suppression by the human von Hippel-Lindau gene product. *Nat Med*. 1995;**1**:822–6.

4. Mandriota SJ, Turner KJ, Davies DR, Murray PG, Morgan NV, Sowter HM, et al. HIF activation identifies early lesions in VHL kidneys: evidence for site-specific tumor suppressor function in the nephron. *Cancer Cell*. 2002;**1**:459–68.

5. Frew IJ, Moch H. A clearer view of the molecular complexity of clear cell renal cell carcinoma. *Annu Rev Pathol*. 2015;**10**:263–89.

6. Frew IJ, Thoma CR, Georgiev S, Minola A, Hitz M, Montani M, et al. pVHL and PTEN tumour suppressor proteins cooperatively suppress kidney cyst formation. *EMBO J*. 2008;**27**:1747–57.

7. Lehmann H, Vicari D, Wild PJ, Frew IJ. Combined Deletion of Vhl and Kif3a Accelerates Renal Cyst Formation. *J Am Soc Nephrol*. 2015;**11**:2778-88.

8. Albers J, Rajski M, Schönenberger D, Harlander S, Schraml P, Teichman von A, et al. Combined mutation of Vhl and Trp53 causes renal cysts and tumours in mice. *EMBO Mol Med*. 2013;**5**:949–64.

9. Wang S-S, Gu Y-F, Wolff N, Stefanius K, Christie A, Dey A, et al. Bap1 is essential for kidney function and cooperates with Vhl in renal tumorigenesis. *Proc Natl Acad Sci USA*. 2014;**111**:16538–43.

10. Maxwell PH, Wiesener MS, Chang GW, Clifford SC, Vaux EC, Cockman ME, et al. The tumour suppressor protein VHL targets hypoxia-inducible factors for oxygen-dependent proteolysis. *Nature*. 1999;**399**:271–5.

11. Yang H, Minamishima YA, Yan Q, Schlisio S, Ebert BL, Zhang X, et al. pVHL Acts as an adaptor to promote the inhibitory phosphorylation of the NF-kappaB agonist Card9 by CK2. *Molecular Cell*. 2007;**28**:15–27.

12. Thoma CR, Frew IJ, Hoerner CR, Montani M, Moch H, Krek W. pVHL and GSK3beta are components of a primary cilium-maintenance signalling network. *Nat Cell Biol*. 2007;**9**:588–95.

13. Roe JS, Kim H, Lee SM, Kim ST, Cho EJ, Youn HD. p53 stabilization and transactivation by a von Hippel-Lindau protein. *Molecular Cell*. 2006;**22**:395–405.

14. Ohh M, Yauch RL, Lonergan KM, Whaley JM, Stemmer-Rachamimov AO, Louis DN, et al. The von Hippel-Lindau tumor suppressor protein is required for proper assembly of an extracellular fibronectin matrix. *Molecular Cell*. 1998;**1**:959–68.

15. Metcalf JL, Bradshaw PS, Komosa M, Greer SN, Meyn MS, Ohh M. K63-

Ubiquitylation of VHL by SOCS1 mediates DNA double-strand break repair. *Oncogene*; 2013;**33**:1055–65.

16. Thoma CR, Toso A, Gutbrodt KL, Reggi SP, Frew IJ, Schraml P, et al. VHL loss causes spindle misorientation and chromosome instability. *Nat Cell Biol*. 2009;**11**:994–1001.

17. Hell MP, Duda M, Weber TC, Moch H, Krek W. Tumor suppressor VHL functions in the control of mitotic fidelity. *Cancer Res*. 2014;**74**:2422–31.

18. Hell MP, Thoma CR, Fankhauser N, Christinat Y, Weber TC, Krek W. miR-28-5p promotes chromosomal instability in VHL-associated cancers by inhibiting Mad2 translation. *Cancer Res*. 2014;**74**:2432–43.

19. Kondo K, Kim WY, Lechpammer M, Kaelin WGJ. Inhibition of HIF2alpha is sufficient to suppress pVHL-defective tumor growth. *PLoS Biology*. 2003;**1**:E83.

20. Raval RR, Lau KW, Tran MG, Sowter HM, Mandriota SJ, Li JL, et al. Contrasting properties of hypoxia-inducible factor 1 (HIF-1) and HIF-2 in von Hippel-Lindau-associated renal cell carcinoma. *Mol Cell Biol*. 2005;**25**:5675–86.

21. Zimmer M, Doucette D, Siddiqui N, Iliopoulos O. Inhibition of hypoxia-inducible factor is sufficient for growth suppression of VHL-/- tumors. *Molecular Cancer Research*. 2004;**2**:89–95.

22. Monzon FA, Alvarez K, Peterson L, Truong L, Amato RJ, Hernandez-McClain J, et al. Chromosome 14q loss defines a molecular subtype of clear-cell renal cell carcinoma associated with poor prognosis. *Mod Pathol*. 2011;**24**:1470–9.

23. Gordan JD, Lal P, Dondeti VR, Letrero R, Parekh KN, Oquendo CE, et al. HIF-alpha effects on c-Myc distinguish two subtypes of sporadic VHL-deficient clear cell renal carcinoma. *Cancer Cell*. 2008;**14**:435–46.

24. Shen C, Beroukhim R, Schumacher SE, Zhou J, Chang M, Signoretti S, et al. Genetic and functional studies implicate HIF1α as a 14q kidney cancer suppressor gene. *Cancer Discov*. 2011;**1**:222–35.

25. Fu L, Wang G, Shevchuk MM, Nanus DM, Gudas LJ. Generation of a Mouse Model of Von Hippel-Lindau Kidney Disease Leading to Renal Cancers by Expression of a Constitutively Active Mutant of HIF1. *Cancer Res*. 2011;**71**:6848–56.

26. Gudas LJ, Fu L, Minton DR, Mongan NP, Nanus DM. The role of HIF1α in renal cell carcinoma tumorigenesis. *J Mol Med*. 2014;**92**:825-36.

27. Iyer NV, Kotch LE, Agani F, Leung SW, Laughner E, Wenger RH, et al. Cellular and developmental control of O2 homeostasis by hypoxia-inducible factor 1 alpha. *Genes & Development*. 1998;**12**:149–62.

28. Papandreou I, Cairns RA, Fontana L, Lim AL, Denko NC. HIF-1 mediates adaptation to hypoxia by actively downregulating mitochondrial oxygen consumption. *Cell Metabolism*. 2006;**3**:187–97.

29. Kim J-W, Tchernyshyov I, Semenza GL, Dang CV. HIF-1-mediated expression of pyruvate dehydrogenase kinase: A metabolic switch required for cellular adaptation to

hypoxia. *Cell Metabolism*. 2006;**3**:177–85.

30. Langbein S, Frederiks WM, Hausen zur A, Popa J, Lehmann J, Weiss C, et al. Metastasis is promoted by a bioenergetic switch: new targets for progressive renal cell cancer. *International Journal of Cancer*. 2008;**122**:2422–8.

31. Luo W, Hu H, Chang R, Zhong J, Knabel M, O'Meally R, et al. Pyruvate kinase M2 is a PHD3-stimulated coactivator for hypoxia-inducible factor 1. *Cell*. 2011;**145**:732–44.

32. Zhang H, Gao P, Fukuda R, Kumar G, Krishnamachary B, Zeller KI, et al. HIF-1 inhibits mitochondrial biogenesis and cellular respiration in VHL-deficient renal cell carcinoma by repression of C-MYC activity. *Cancer Cell*. 2007;**11**:407–20.

33. Metallo CM, Gameiro PA, Bell EL, Mattaini KR, Yang J, Hiller K, et al. Reductive glutamine metabolism by IDH1 mediates lipogenesis under hypoxia. *Nature*. 2012;**481**:380–4.

34. Chan DA, Sutphin PD, Nguyen P, Turcotte S, Lai EW, Banh A, et al. Targeting GLUT1 and the Warburg effect in renal cell carcinoma by chemical synthetic lethality. *Science Translational Medicine*. 2011;**3**:94ra70.

35. Sun RC, Denko NC. Hypoxic regulation of glutamine metabolism through HIF1 and SIAH2 supports lipid synthesis that is necessary for tumor growth. *Cell Metabolism*. 2014;**19**:285–92.

36. Tello D, Balsa E, Acosta-Iborra B, Fuertes-Yebra E, Elorza A, Ordóñez A, et al. Induction of the Mitochondrial NDUFA4L2 Protein by HIF-1a Decreases Oxygen Consumption by Inhibiting Complex I Activity. *Cell Metabolism*. 2011;**14**:768–79.

37. Fukuda R, Zhang H, Kim J-W, Shimoda L, Dang CV, Semenza GL. HIF-1 regulates cytochrome oxidase subunits to optimize efficiency of respiration in hypoxic cells. *Cell*. 2007;**129**:111–22.

38. Li B, Qiu B, Lee DSM, Walton ZE, Ochocki JD, Mathew LK, et al. Fructose-1,6-bisphosphatase opposes renal carcinoma progression. *Nature*. 2014;**513**:251-5.

39. Cancer Genome Atlas Research Network. Comprehensive molecular characterization of clear cell renal cell carcinoma. *Nature*. 2013;**499**:43–9.

40. Ryan HE, Poloni M, McNulty W, Elson D, Gassmann M, Arbeit JM, et al. Hypoxia-inducible factor-1alpha is a positive factor in solid tumor growth. *Cancer Res*. 2000;**60**:4010–5.

41. Gruber M, Hu C-J, Johnson RS, Brown EJ, Keith B, Simon MC. Acute postnatal ablation of Hif-2alpha results in anemia. *Proc Natl Acad Sci USA*. 2007;**104**:2301–6.

42. Shao X, Somlo S, Igarashi P. Epithelial-specific Cre/lox recombination in the developing kidney and genitourinary tract. *J Am Soc Nephrol*. 2002;**13**:1837–46.

43. Zhang H, Bosch-Marce M, Shimoda LA, Tan YS, Baek JH, Wesley JB, et al. Mitochondrial Autophagy Is an HIF-1-dependent Adaptive Metabolic Response to Hypoxia. *Journal of Biological Chemistry*. 2008;**283**:10892–903.

44. Rankin EB, Tomaszewski JE, Haase VH. Renal cyst development in mice with

conditional inactivation of the von Hippel-Lindau tumor suppressor. *Cancer Res*. 2006;**66**:2576–83.

45. Pritchett TL, Bader HL, Henderson J, Hsu T. Conditional inactivation of the mouse von Hippel-Lindau tumor suppressor gene results in wide-spread hyperplastic, inflammatory and fibrotic lesions in the kidney. *Oncogene*. 2014;**34**:2631–9.

46. Adam J, Hatipoglu E, O'Flaherty L, Ternette N, Sahgal N, Lockstone H, et al. Renal cyst formation in Fh1-deficient mice is independent of the Hif/Phd pathway: roles for fumarate in KEAP1 succination and Nrf2 signaling. *Cancer Cell*. 2011;**20**:524–37.

47. Schietke RE, Hackenbeck T, Tran M, Günther R, Klanke B, Warnecke CL, et al. Renal tubular HIF-2α expression requires VHL inactivation and causes fibrosis and cysts. *PloS One*. 2012;**7**:e31034.

48. Fu L, Wang G, Shevchuk MM, Nanus DM, Gudas LJ. Activation of HIF2 in Kidney Proximal Tubule Cells Causes Abnormal Glycogen Deposition but not Tumorigenesis. *Cancer Res*. 2013;**73**:2916–25.

49. LaGory EL, Wu C, Taniguchi CM, Ding C-KC, Chi J-T, Eyben von R, et al. Suppression of PGC-1a Is Critical for Reprogramming Oxidative Metabolism in Renal Cell Carcinoma. *Cell Reports*. 2015;**12**:116-27.

50. Koh MY, Nguyen V, Lemos R, Darnay BG, Kiriakova G, Abdelmelek M, et al. Hypoxia-induced SUMOylation of E3 ligase HAF determines specific activation of HIF2 in clear-cell renal cell carcinoma. *Cancer Res*. 2015;**75**:316–29.

| | $Vhl^{\Delta/\Delta}Trp53^{\Delta/\Delta}$ | $Vhl^{\Delta/\Delta}Trp53^{\Delta/\Delta}Hif1a^{\Delta/\Delta}$ | $Vhl^{\Delta/\Delta}Trp53^{\Delta/\Delta}Hif2a^{\Delta/\Delta}$ |
|---|---|---|---|
| Number of renal cysts | 399 (n=30 kidneys) | 15 (n=30 kidneys) | 10 (n=22 kidneys) |
| Number of renal tumors | 16 (n=30 kidneys) | 0 (n=30 kidneys) | 0 (n=22 kidneys) |
| Number of genital-urinary tract carcinomas | 6 (n=17 mice) | 0 (n=15 mice) | 0 (n=18 mice) |
| Incidence of epididymal dysplasia/squamous metaplasia | 100% (n=9 mice) | 0% (n=7 mice) | 50% (n=8 mice) |
| Incidence of seminal vesicle abnormality | 100% (n=9 mice) | 0% (n=7 mice) | 100% (n=8 mice) |

**Table 1:** Summary of phenotypes in $Vhl^{\Delta/\Delta}Trp53^{\Delta/\Delta}$, $Vhl^{\Delta/\Delta}Trp53^{\Delta/\Delta}Hif1a^{\Delta/\Delta}$ and $Vhl^{\Delta/\Delta}Trp53^{\Delta/\Delta}Hif2a^{\Delta/\Delta}$ mice aged 11 to 13 months. Numbers of renal cysts and renal tumours are derived from analysis of midline longitudinal sections of n kidneys of each genotype. Numbers of genital-urinary tract carcinomas represent the cumulative number of tumors arising in the epididymis, seminal vesicle, uterus and urothelium of n mice of each genotype. The incidence of epididymal and seminal vesicle phenotypes represents the % of n mice of each genotype that display the listed phenotypes.

**FIGURE LEGENDS**

**Figure 1. Renal epithelial cell-specific deletion of *Vhl*, *Hif1a, Hif2a, Vhl/Hif1a* and *Vhl/Hif2a*.**
H&E stainings of renal cortex (A) and medulla (B) and immunohistochemical stainings for HIF-1α (C), HIF-2α (D) and GLUT1 (E) in the renal cortex.

**Figure 2. Deletion of *Vhl/Trp53*, *Vhl/Trp53/Hif1a* and *Vhl/Trp53/Hif2a* in renal epithelial cells.**
(A,B) H&E stainings of renal cortex from mice aged 6 months (A) and 12 months (B). Arrowheads highlight disorganized tubules with clear cell cytoplasm and arrows highlight optically-clear nuclei, Cy labels cysts and Neo labels a neoplasm. Immunohistochemical stainings for HIF-1α (C), HIF-2α (D) and GLUT1 (E) in the renal cortex. (F) H&E stainings of vesicular glands from mice aged 6 months. (G,H) H&E stainings of epididymides from mice aged 12 months.

**Figure 3. Control of renal epithelial cell proliferation by HIF-1α and HIF-2α.**
(A,B) Ki67 staining of renal cortices of 6 month-old (A) or 12 month-old (B) mice. (C,D) Ki67 positive tubular epithelial cells per field (0.36 $mm^2$) in 6 month-old (C) or 12 month-old (D) mice. Mean ± SEM from 5 separate regions in 3-5 kidneys of each genotype.

**Figure 4. HIF-1α stabilization inhibits mitochondrial oxidation in *Vhl*-deficient cells**
(A) Workflow for microarray analysis of mRNA expression 4 days after deletion of *Vhl* alone or together with *Hif1a* and/or *Hif2a* in primary renal epithelial cells. (B) Gene expression clustering of differentially expressed genes between Adeno-Cre and Adeno-GFP-treated cells. Rows represent mean $log_2$ ratios values of 3 independent samples of each genotype. HIF-1α-specific or HIF-2α-specific target genes or genes that are regulated by both HIF-1α and HIF-2 α are indicated. (C) Heat map of gene expression of HIF-1α-specific genes. (D) mRNA abundance of the indicated genes in kidneys deficient for *Vhl*, *Vhl/Hif1a* and *Vhl/Hif2a*. Mean ± std. dev. (n = 6 mice of each

genotype) gene expression ratios between Ksp1.3-Cre and wild type (WT) mice, normalized to expression of *Rps12*. (E) Respirometry of biopsies from cortex and medulla of wild type (+/+, black bars) and knockout (Ksp1.3-Cre/+, white bars) genotypes (n = 6 mice per genotype) in $Vhl^{fl/fl}$ (left column), $Vhl^{fl/fl}Hif1a^{fl/fl}$ (middle column) and $Vhl^{fl/fl}Hif2a^{fl/fl}$ (right column) kidneys. Graphs depict oxygen consumption attributable to total ATP synthase capacity, complex I, complex II, complex IV and medium chain fatty acid oxidation.

**Figure 5**. **Cellular metabolic phenotypes in *Vhl*, *Vhl/Hif1a* and *Vhl/Hif2a* deficient mice.**

(A-H) Immunofluorescence stainings for AQP2, TOM20 and DAPI. A-D shows overlaid channels, E-H shows TOM20 fluorescence only, arrowheads highlight examples of collecting duct principal cells. (I-L) H&E staining of renal cortex. Arrowheads highlight epithelial cells with clear cell cytoplasm and arrows highlight optically-clear nuclei. (M-P) Periodic acid-Schiff (PAS) staining of the renal cortex. Arrows highlight optically clear nuclei that display strong accumulation of glycogen. (Q-T) Oil red O staining in the renal cortex. (U) Average TOM20 intensity in AQP2 positive cells. 43-64 tubules were analysed in 7-11 separate regions per genotype. (V) Oil red O staining of peri-renal fat. (W) mRNA abundance of the indicated genes in kidneys deficient for *Vhl*, *Vhl/Hif1a* and *Vhl/Hif2a* (n = 6 mice of each genotype) of the ratios of gene expression between Ksp1.3-Cre and wild type (WT) mice, normalized to expression of *Rps12*.

**Figure 6**. **Impact of *Vhl*, *Hif1a*, *Hif2a* and *Trp53* mutations on glycolysis, oxygen consumption and ATP production.**

(A) mRNA abundance of the indicated genes between Adeno-Cre and Adeno-GFP treated MEFs (72 hours after infection), normalized to expression of *Rps12* (n=3). (B) Relative glucose utilization, (C) extracellular acidification rate (ECAR), (D) relative lactate production, (E) oxygen consumption rate (OCR) of Adeno-GFP or Adeno-Cre treated cultures of MEFs 72 hours after infection. B and D show pooled data from 3 independent experiments each assayed in quadruplicate

and C and E depict single representative experiments of 3 independent experiments each involving 5 replicate assays per genotype. (F) Flow cytometry using 10-N-Nonyl acridine orange (NAO) staining. Filled grey curves show Adeno-GFP infected cells, non-filled curves show Adeno-Cre infected cells (G,H) Relative cellular ATP levels of Adeno-GFP and Adeno-Cre treated cells of the indicated genotypes. n=11-30 independent experiments, each with 3-5 technical replicates.

**Figure 1**

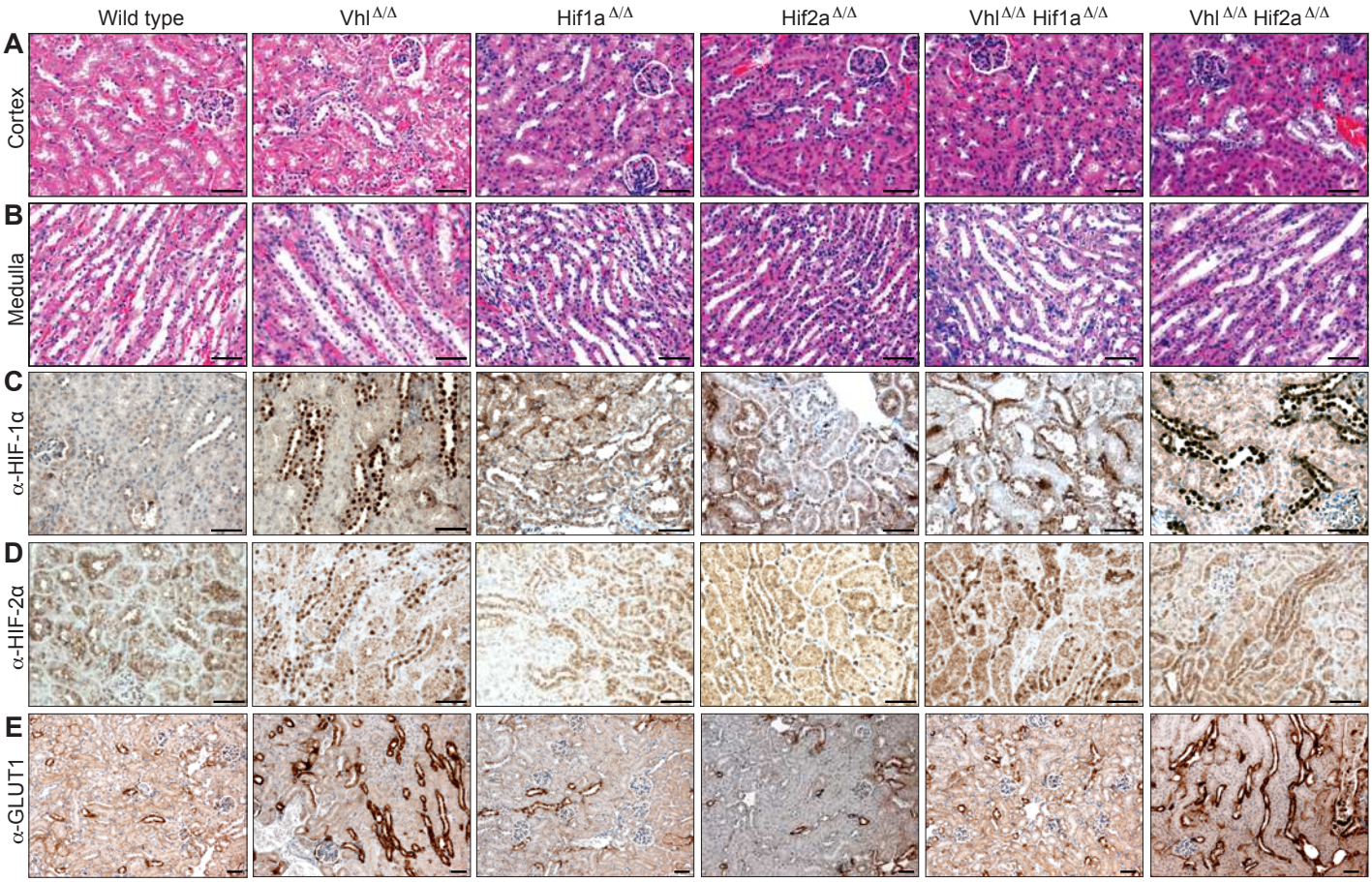
Wild type
Vhl Δ/Δ
Hif1a Δ/Δ
Hif2a Δ/Δ
Vhl Δ/Δ Hif1a Δ/Δ
Vhl Δ/Δ Hif2a Δ/Δ
A
Cortex
B
Medulla
C
α-HIF-1α
D
α-HIF-2α
E
α-GLUT1

Figure 2

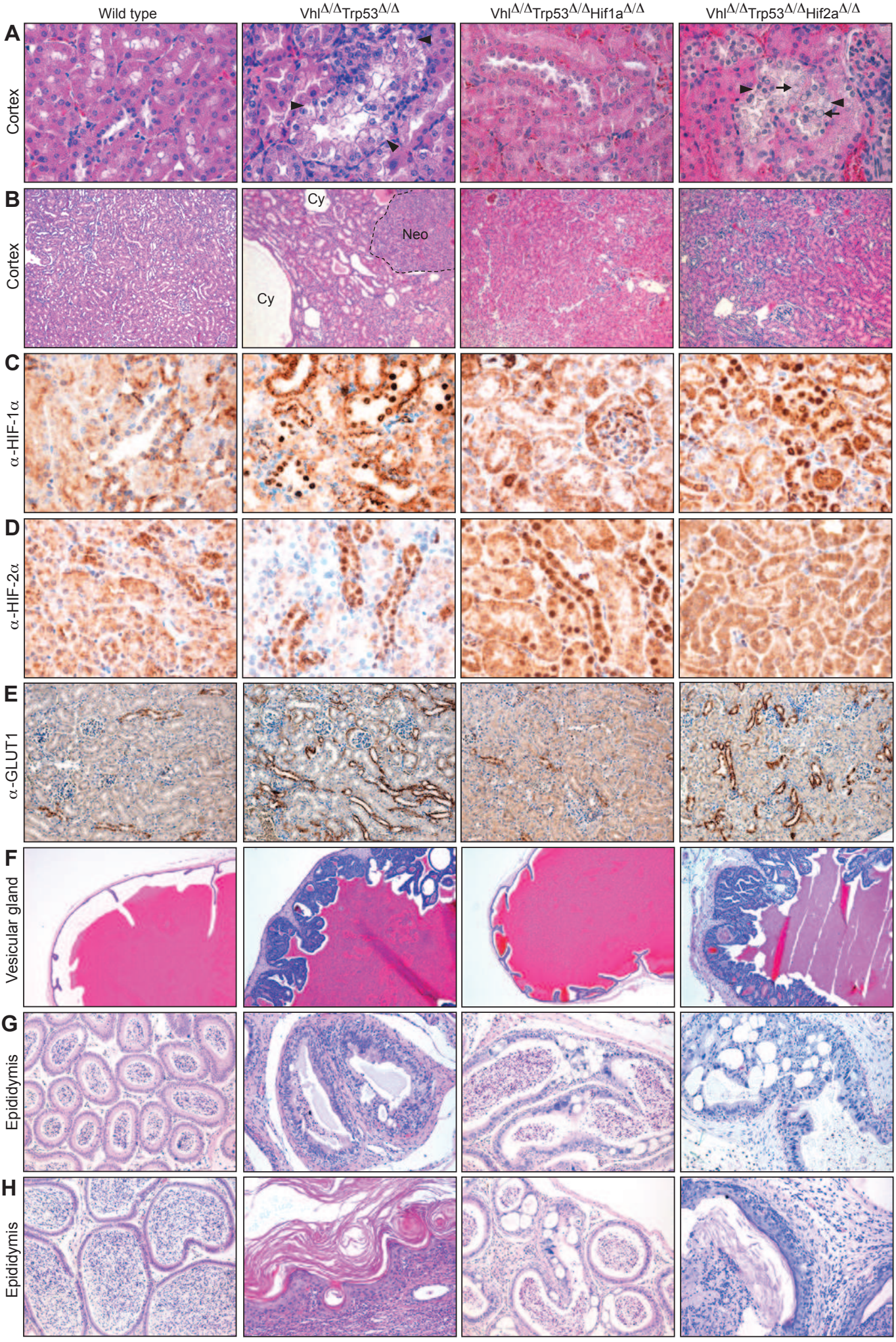
Wild type
Vhl$^{\Delta/\Delta}$Trp53$^{\Delta/\Delta}$
Vhl$^{\Delta/\Delta}$Trp53$^{\Delta/\Delta}$Hif1a$^{\Delta/\Delta}$
Vhl$^{\Delta/\Delta}$Trp53$^{\Delta/\Delta}$Hif2a$^{\Delta/\Delta}$
A
Cortex
B
Cortex
Cy
Neo
Cy
C
α-HIF-1α
D
α-HIF-2α
E
α-GLUT1
F
Vesicular gland
G
Epididymis
H
Epididymis

**Figure 3**

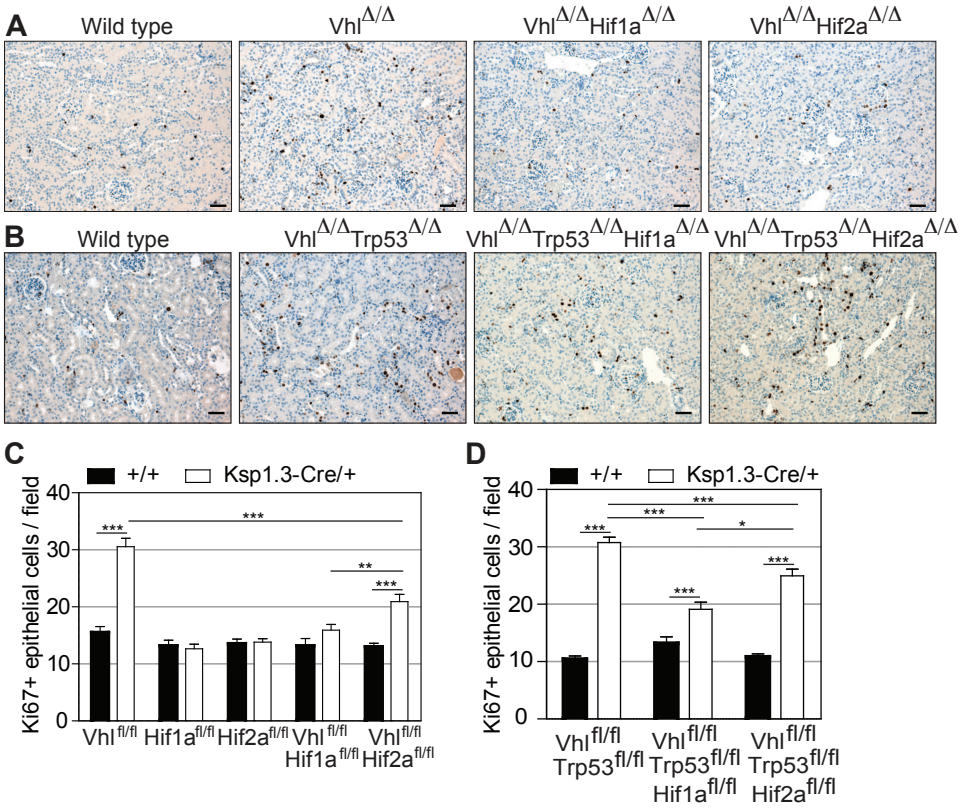
A
Wild type
Vhl$^{\Delta/\Delta}$
Vhl$^{\Delta/\Delta}$Hif1a$^{\Delta/\Delta}$
Vhl$^{\Delta/\Delta}$Hif2a$^{\Delta/\Delta}$
B
Wild type
Vhl$^{\Delta/\Delta}$Trp53$^{\Delta/\Delta}$
Vhl$^{\Delta/\Delta}$Trp53$^{\Delta/\Delta}$Hif1a$^{\Delta/\Delta}$
Vhl$^{\Delta/\Delta}$Trp53$^{\Delta/\Delta}$Hif2a$^{\Delta/\Delta}$
C
+/+
Ksp1.3-Cre/+
Ki67+ epithelial cells / field
0
10
20
30
40
***
***
**
***
Vhl$^{fl/fl}$
Hif1a$^{fl/fl}$
Hif2a$^{fl/fl}$
Vhl$^{fl/fl}$ Hif1a$^{fl/fl}$
Vhl$^{fl/fl}$ Hif2a$^{fl/fl}$
D
+/+
Ksp1.3-Cre/+
Ki67+ epithelial cells / field
0
10
20
30
40
***
***
*
***
***
Vhl$^{fl/fl}$ Trp53$^{fl/fl}$
Vhl$^{fl/fl}$ Trp53$^{fl/fl}$ Hif1a$^{fl/fl}$
Vhl$^{fl/fl}$ Trp53$^{fl/fl}$ Hif2a$^{fl/fl}$

**Figure 4**

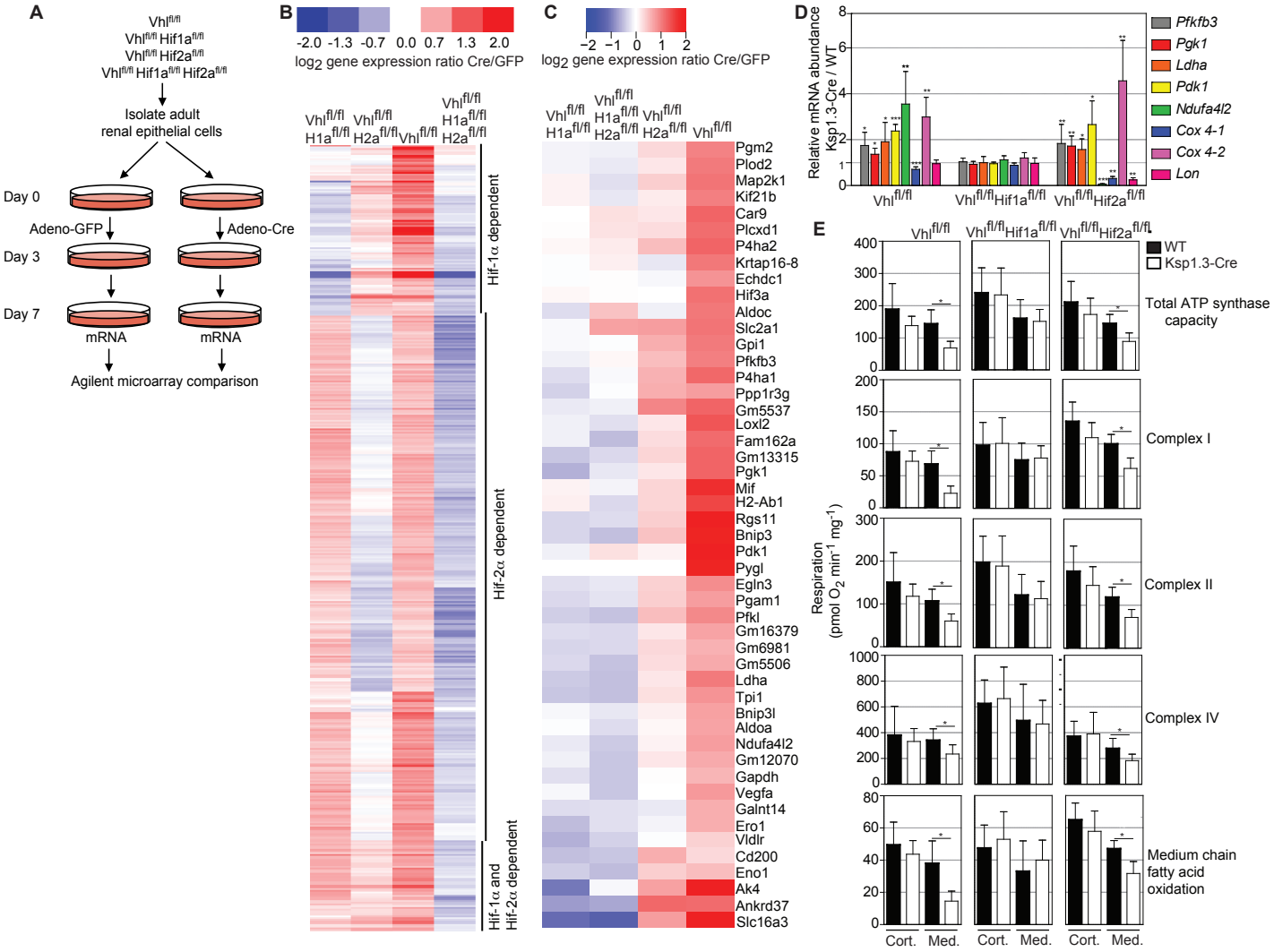
A
Vhl fl/fl
Vhl fl/fl Hif1a fl/fl
Vhl fl/fl Hif2a fl/fl
Vhl fl/fl Hif1a fl/fl Hif2a fl/fl
Isolate adult renal epithelial cells
Day 0
Adeno-GFP
Adeno-Cre
Day 3
Day 7
mRNA
mRNA
Agilent microarray comparison
B
-2.0 -1.3 -0.7 0.0 0.7 1.3 2.0
log2 gene expression ratio Cre/GFP
Vhl fl/fl H1a fl/fl
Vhl fl/fl H2a fl/fl
Vhl fl/fl
Vhl fl/fl H1a fl/fl H2a fl/fl
Hif-1α dependent
Hif-2α dependent
Hif-1α and Hif-2α dependent
C
−2 −1 0 1 2
log2 gene expression ratio Cre/GFP
Vhl fl/fl H1a fl/fl
Vhl fl/fl H1a fl/fl H2a fl/fl
Vhl fl/fl H2a fl/fl
Vhl fl/fl
Pgm2
Plod2
Map2k1
Kif21b
Car9
Plcxd1
P4ha2
Krtap16-8
Echdc1
Hif3a
Aldoc
Slc2a1
Gpi1
Pfkfb3
P4ha1
Ppp1r3g
Gm5537
Loxl2
Fam162a
Gm13315
Pgk1
Mif
H2-Ab1
Rgs11
Bnip3
Pdk1
Pygl
Egln3
Pgam1
Pfkl
Gm16379
Gm6981
Gm5506
Ldha
Tpi1
Bnip3l
Aldoa
Ndufa4l2
Gm12070
Gapdh
Vegfa
Galnt14
Ero1
Vldlr
Cd200
Eno1
Ak4
Ankrd37
Slc16a3
D
Relative mRNA abundance Ksp1.3-Cre / WT
Vhl fl/fl
Vhl fl/fl Hif1a fl/fl
Vhl fl/fl Hif2a fl/fl
Pfkfb3
Pgk1
Ldha
Pdk1
Ndufa4l2
Cox 4-1
Cox 4-2
Lon
E
Vhl fl/fl
Vhl fl/fl Hif1a fl/fl
Vhl fl/fl Hif2a fl/fl
WT
Ksp1.3-Cre
Total ATP synthase capacity
Complex I
Complex II
Complex IV
Medium chain fatty acid oxidation
Respiration (pmol O2 min-1 mg-1)
Cort.
Med.

**Figure 5**

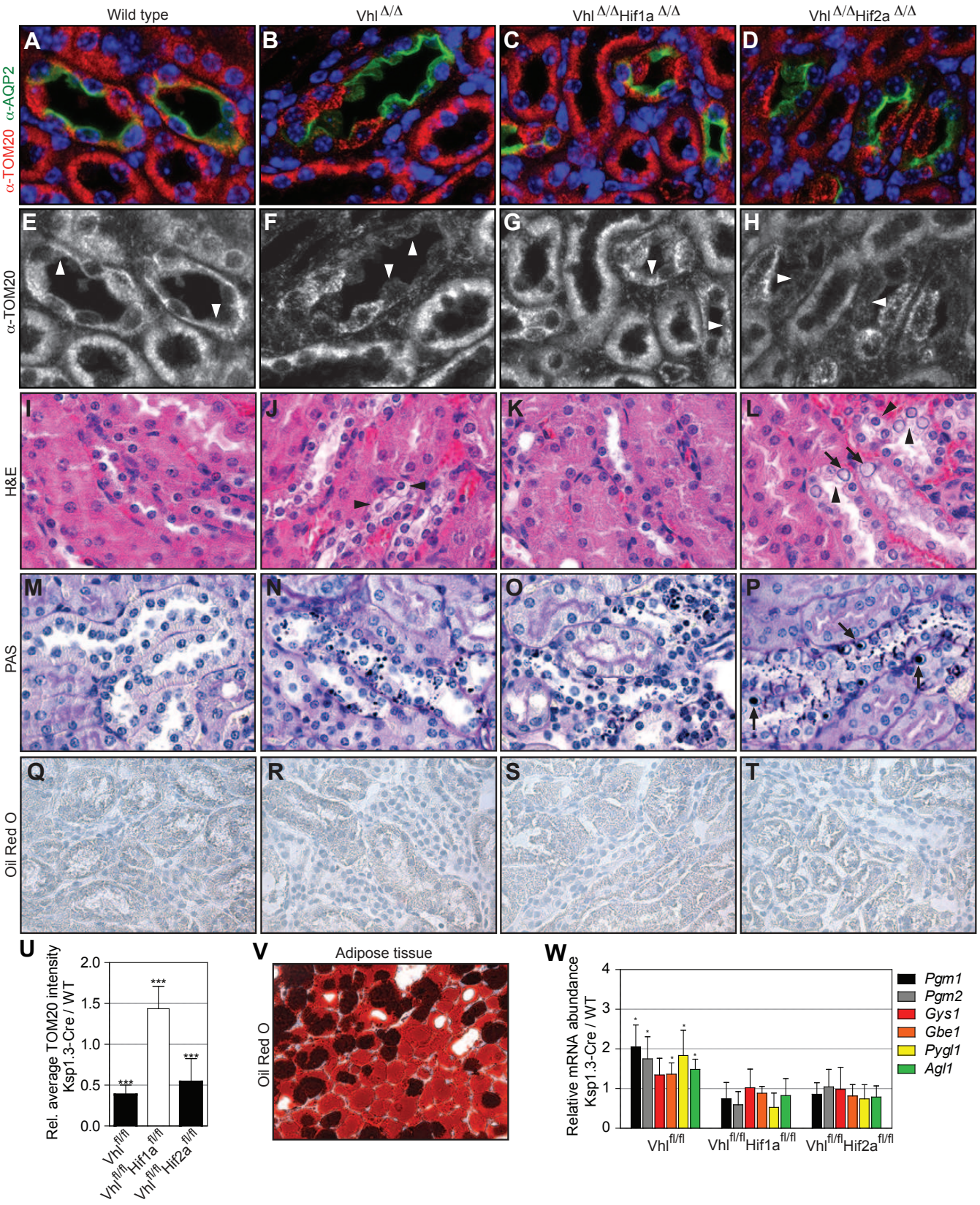
Wild type
Vhl Δ/Δ
Vhl Δ/ΔHif1a Δ/Δ
Vhl Δ/ΔHif2a Δ/Δ
α-TOM20 α-AQP2
α-TOM20
H&E
PAS
Oil Red O
A
B
C
D
E
F
G
H
I
J
K
L
M
N
O
P
Q
R
S
T
U
Rel. average TOM20 intensity Ksp1.3-Cre / WT
2.0
1.5
1.0
0.5
0.0
***
Vhl fl/fl
Vhl fl/fl Hif1a fl/fl
Vhl fl/fl Hif2a fl/fl
V
Adipose tissue
Oil Red O
W
Relative mRNA abundance Ksp1.3-Cre / WT
4
3
2
1
0
Vhl fl/fl
Vhl fl/fl Hif1a fl/fl
Vhl fl/fl Hif2a fl/fl
Pgm1
Pgm2
Gys1
Gbe1
Pygl1
Agl1

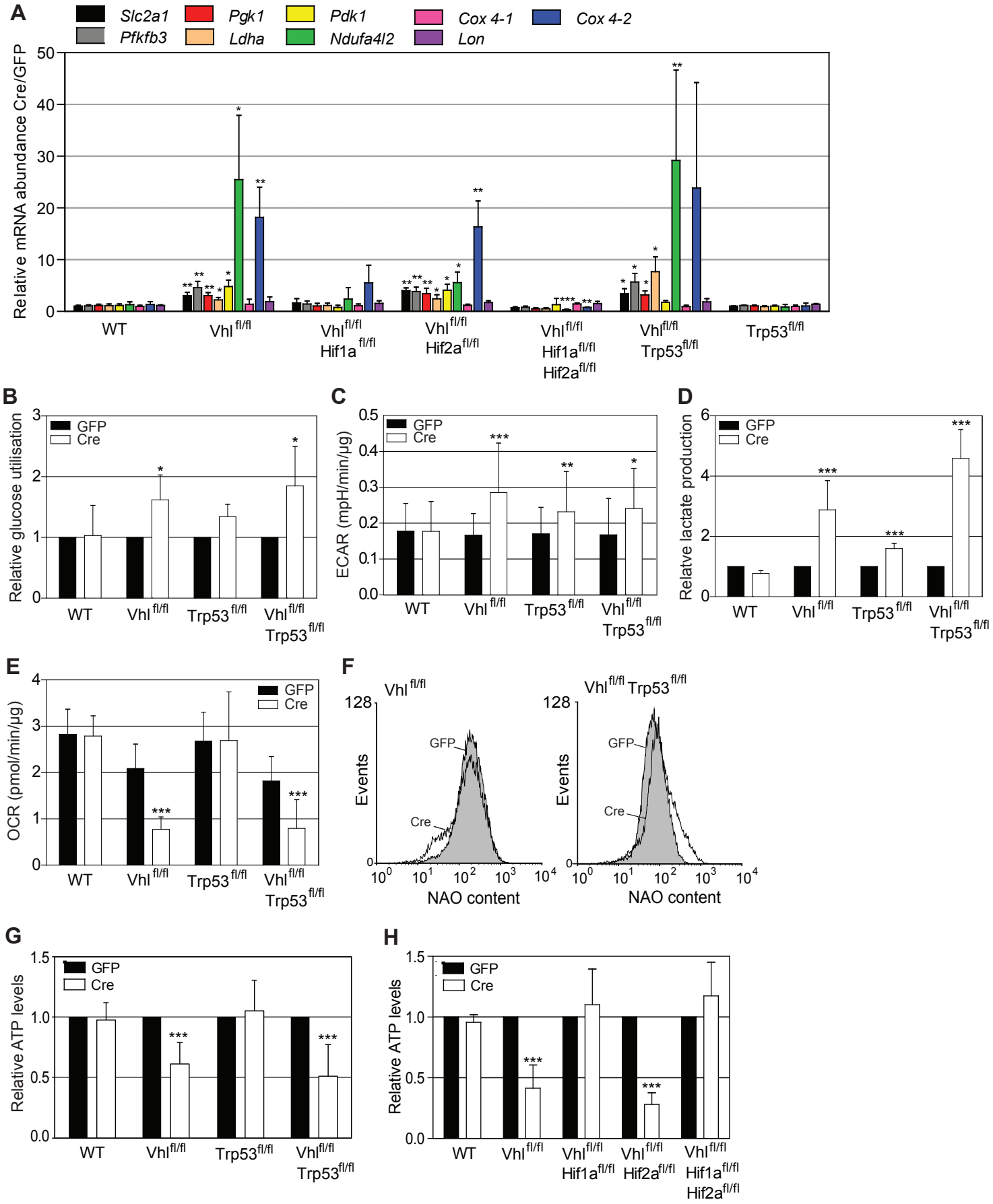
A
Slc2a1
Pfkfb3
Pgk1
Ldha
Pdk1
Ndufa4l2
Cox 4-1
Lon
Cox 4-2
Relative mRNA abundance Cre/GFP
WT
Vhl fl/fl
Vhl fl/fl Hif1a fl/fl
Vhl fl/fl Hif2a fl/fl
Vhl fl/fl Hif1a fl/fl Hif2a fl/fl
Vhl fl/fl Trp53 fl/fl
Trp53 fl/fl
B
Relative glucose utilisation
GFP
Cre
Vhl fl/fl Trp53 fl/fl
C
ECAR (mpH/min/µg)
D
Relatve lactate production
E
OCR (pmol/min/µg)
F
Events
NAO content
G
Relative ATP levels
H
Relative ATP levels